ACS APPLIED MATERIALS & INTERFACES

Letter

www.acsami.org

Growth and Bending-Sensitive Photoluminescence of a Flexible $PbTiO_3$/ZnO Nanocomposite

Shan Jiang, Zhaohui Ren,* Simin Yin, Siyu Gong, Yifeng Yu, Xiang Li, Xiao Wei, Gang Xu, Ge Shen, and Gaorong Han*

State Key Laboratory of Silicon Materials, Department of Materials Science and Engineering, Cyrus Tang Center for Sensor Materials and Application, Zhejiang University, Hangzhou 310027, P. R. China

Supporting Information

ABSTRACT: A brushlike $PbTiO_3$ (PTO)/ZnO nanocomposite with ZnO nanowires (NWs) grown epitaxially on the surface of single-crystal ferroelectric tetragonal PTO NWs is successfully fabricated onto a flexible substrate via a two-step hydrothermal process. In this nanocomposite, a ZnO NW grew along [0001] on the (101) plane of the core PTO NW with a lattice mismatch of 1.06% to form an effective ferroelectric/semiconductor interface. It is found that the ultraviolet photoluminescence emission of the nanocomposite could be easily tuned by its bending curvatures at room temperature. This intriguing phenomenon can be understood by the bending-induced polarization field from the PTO NW, which could reduce the bending degree of the energy band of the ZnO NWs through the interface. Throughthe design of an effective interface, this kind of ferroelectric/semiconductor nanocomposite may find potential applications in sensor and piezophotonic nanodevices.

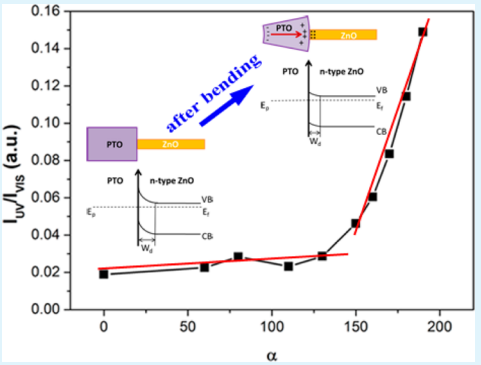

KEYWORDS: *photoluminescence, lead titanate, zinc oxide, flexible nanocomposites*

INTRODUCTION

One-dimensional (1D) nanomaterials, such as nanorods, nanowires (NWs), and nanotubes, have been the focus of numerous studies to develop nanoscale and microscale technologies.[1,2] As a typical wide-band-gap (3.3 eV) semiconductor, ZnO NW is demonstrated as an ideal building block for fabricating various potential optoelectronic devices.[3−6] Coupled with semiconducting properties, its piezoelectric effect was explored to produce novel flexible nanodevices, such as nanogenerators,[7−9] sensors,[10−12] and piezoelectric field-effect transistors.[13] Recently, a flexible strain sensor has been achieved on the basis of the piezoelectric nanocomposite material with ZnO nanostructures embedded in a stable matrix of paper.[14] Besides, to improve the electromechanical coupling performance of the devices, perovskite-type ferroelectric PZT and other piezoelectric materials with larger piezoelectric coefficients have also been investigated.[15,16] Over the past decades, 1D perovskite ferroelectric nanomaterials have been extensively explored because of their intriguing ferroelectric and piezoelectric properties, such as vortex polarization, which pave the way for promising application from nanogenerators to ultrahigh-density memories.[17−20] In addition to their intrinsic properties, it was discovered that the reversed polarization direction by an external electric field played a key role in determining the transport property of the ferroelectric materials.[21] For example, the ferroelectric polarization in single-domain $BiFeO_3$ crystals has been shown to switch the photocurrent created by ultraviolet (UV)-light illumination.[22] In the metal/ferroelectric/semiconductor heterostructures, the ferroelectric polarization has been determined to have an effect on the height and width of the barrier at the interface, resulting in corresponding low and high resistance states of the system.[23] These important achievements encourage us to design a nanoscaled ferroelectric/semiconductor heterostructure, where some fascinating properties may be involved via the added piezophotonic coupling at the interface.

Among ferroelectric oxides, lead titanate ($PbTiO_3$ or PTO) is a typical material for its simple structure and very large spontaneous polarization.[24] In particular, a single-crystal PTO NW, as a potential candidate for high-performance piezoelectric application, has been reported numerously for its crystal structure, doping modification, and ferroelectric phase transformation in our preview work.[25−27] Combined with the facile preparation of ZnO NW, we proposed the design of a flexible nanocomposite with ZnO NW grown on the surface of a perovskite PTO NW via a two-step hydrothermal method. In this work, we report for the first time a high lattice match degree of a single-crystal ferroelectric/semiconductor interface at nanoscale. Interestingly, the photoluminescence (PL) properties of the nanocomposite can be easily tuned by bending-induced polarization effects at the interface, which could be useful for the design and fabrication of piezophotonic nanodevices.

Received: February 12, 2014
Accepted: July 1, 2014
Published: July 1, 2014

EXPERIMENTAL SECTION

Single-crystal perovskite PTO NW powders were prepared via a polymer-assisted hydrothermal method reported in our preview work.[28] The ZnO NWs were grown on PTO NWs through embedding ZnO seeds onto PTO NWs, followed by a hydrothermal process.[29,30] The experimental details were listed in the Supporting Information (SI).

The morphology and crystalline structure of the as-prepared PTO/ZnO nanocomposite were characterized by a Hitachi field-emission scanning electron microscopy (FESEM; model S-4800) at 5 kV and high-resolution transmission electron microscopy (HRTEM; JEM 2010F) at 200 kV. Powder X-ray diffraction (XRD) patterns were collected at room temperature on a Thermo ARL X'TRA powder diffractometer with Bragg–Brentano geometry by Cu K α radiation (λ = 1.54056 Å) with 0.82 Å resolution. The PL measurement of the PTO/ZnO-nanocomposite-covered substrates bent to various curvatures was performed at room temperature using the 325 nm line of a continuous-wave He–Cd laser as the excitation source.

RESULTS AND DISCUSSION

Figure 1 illustrates the fabrication principle of the PTO/ZnO nanocomposite. Such a layer of ZnO nanoparticle seeds with

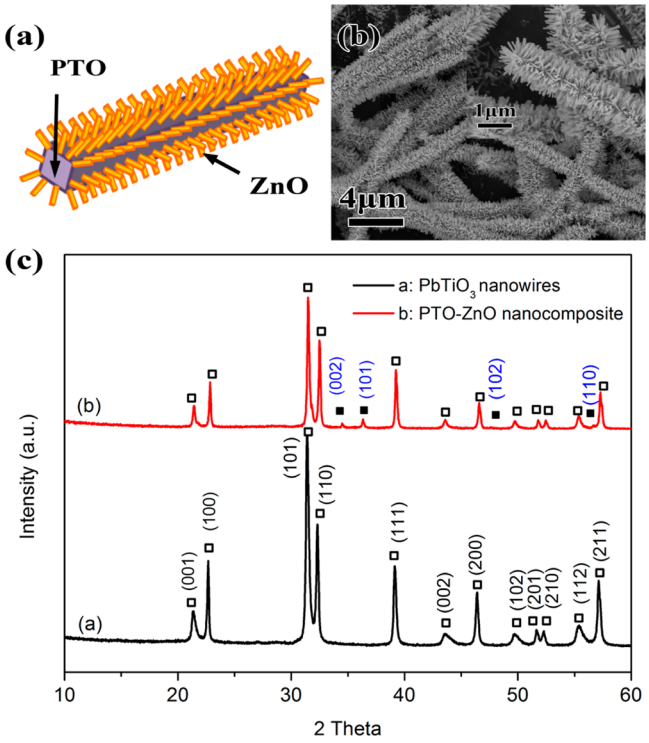

Figure 1. (a) Schematic depiction of the fabrication of a PTO/ZnO nanocomposite. (b) SEM image of a typical PTO/ZnO brushlike nanocomposite. The inset shows a high-resolution SEM image of the composite. (c) XRD patterns of the PTO NWs (curve a) and PTO/ZnO nanocomposite (curve b): (■) wurtzite phase of ZnO; (□) tetroagnal peroskite phase of PTO.

diameters of 5–10 nm on the surface of PTO NWs can be observed from the scanning electron microscopy (SEM) image (Figure S2 in the SI). It is noted that the seed layer is necessary because the PTO/ZnO nanocomposite cannot be attained when this step is omitted (Figure S3 in the SI). Then ZnO NWs are sprouted from the ZnO seeds by a simple hydrothermal process (Figure 1a).[30] The SEM images of the ZnO NWs growing on PTO NWs are shown in Figure 1b. It is clear that ZnO NWs, whose diameter and length are about 50 nm and 1 μm, respectively, dispersed around the surface of PTO NWs to form a ZnO/PTO nanocomposite (inset of Figure 1b). Figure 1c illustrates the XRD patterns of the core PTO NWs (curve a) and composites (curve b) as a comparison. Clearly, the crystal phase of PTO used as the primary core material is tetragonal perovskite (JCPDS: 06-0452). For the PTO/ZnO nanocomposite, all of the diffraction peaks can be indexed as a combination of hexagonal wurtzite ZnO (JCPDS: 036-1451) and the tetragonal perovskite PTO.

The hybrid structure was further examined using transmission electron microscopy (TEM). The TEM image in Figure 2a shows a portion of the PTO/ZnO nanocomposite. It is noted that some branches were broken off from the surface of the core PTO NW by sonication during the TEM sample preparation process. A partial lattice image of branch ZnO NWs can be observed in the inset of Figure 2a, and its corresponding diffraction pattern obtained by fast Fourier transform (FFT) along the [0010] zone axis is shown in Figure 2c. The 0.260 and 0.281 nm interval of the lattice fringes detected in the image agree well with the spacing of the planes of (0001) and (1000), separately. These results identify that the single-crystal ZnO grows along the [0001] axis with surfaces enclosed by the {1000} plane. Figure 2b displays the interface region of one branch, from which the HRTEM image was achieved. Both the branch and core are single crystalline with clear lattice fringes. The lattice spacing of 0.284 and 0.390 nm for the core can be indexed into the (010) and (101) planes of tetragonal perovskite PTO. Besides, the single-crystal perovskite PTO NW was determined to grow along the [001] axis with surfaces enclosed by the {100} plane according to our preview work.[28] Parts d and e of Figure 2 show the FFT pattern of the lattice image of the interface and the core PTO, suggesting that there is an interfacial relationship between the (1000) plane of ZnO and the (101) plane of PTO. In our experiment, the lattice mismatch at the hybrid interfaces was evaluated to be 1.06% along the [010] direction of PTO. The low lattice mismatch is highly beneficial to the nucleation and growth of the branch ZnO NWs on the PTO NWs by reducing the structural strain in the epitaxial growth of heterogeneous structures by solution-phase growth.[30] As a result, the ZnO nanocrystals, which tend to elongate along the [0001] direction during solution growth, prefer to nucleate and grow on the {010} planes of PTO NWs, leading to the formation of a brushlike nanocomposite.

To better understand the growth of the ZnO NWs on the surface of PTO NWs, the effect of the growth time was investigated. Parts a–e of Figure 3 show the representative SEM images of the PTO/ZnO nanocomposite after different reaction times of 0.5, 1, 2, 4, and 6 h, respectively. With a short growth of 0.5 h, some thin and sparse ZnO NWs began to sprout from the seeds (Figure 3a). When the reaction time is at 1 h, the ZnO NWs vertically oriented on the surface of the PTO cores became longer and denser, as shown in Figure 3b. It should also be noticed that the nanocomposite has brushlike morphology. With a further increase of the reaction time from 2 to 6 h, increases in the diameter, length, and density of the ZnO NW branches (Figure 3c–e) can be observed. The diameter and length of the ZnO NWs varied in the ranges of 30–200 and 200–2000 nm, respectively. Therefore, in our experiment, the morphology of the ZnO nanostructures can be easily tailored by the growth duration. Furthermore, as shown in the cross-sectional SEM image (Figure 3f), the core PTO NW lies flat on the flexible substrate, where ZnO NWs were

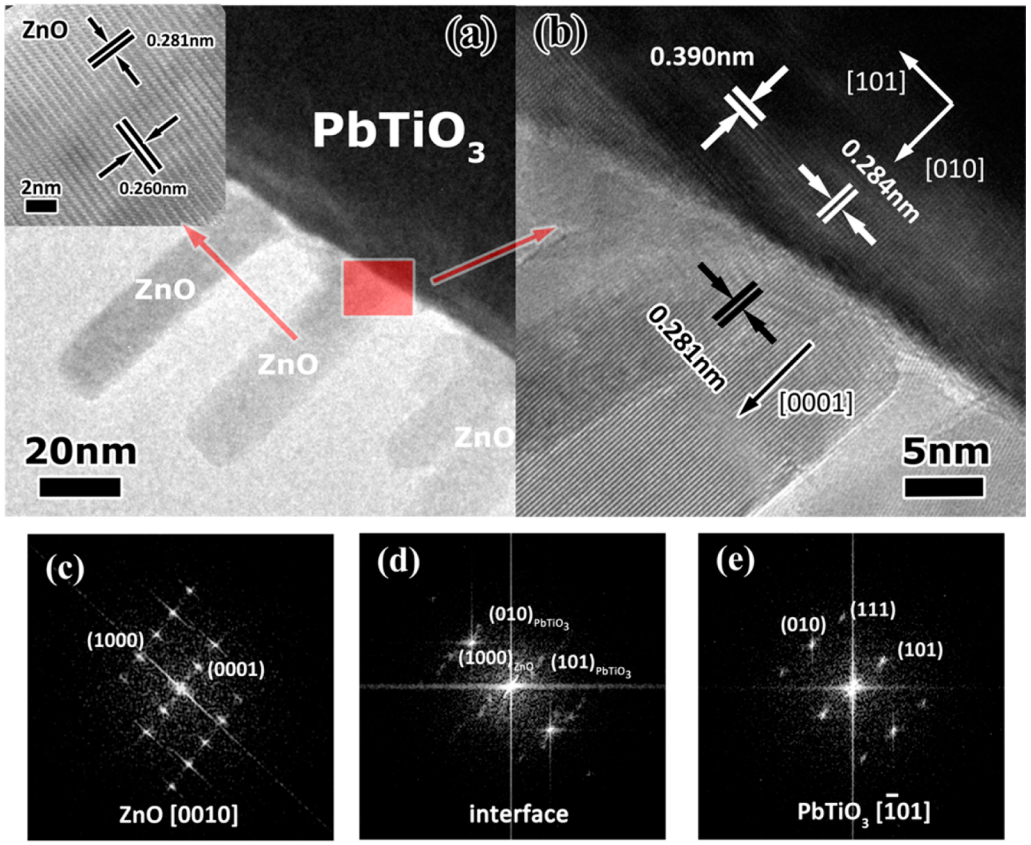

Figure 2. Microstructural characterization of the heterointerface. (a) TEM image of the partial PTO/ZnO NW. The inset shows the HRTEM image of the ZnO branch. (b) HRTEM image of the PTO/ZnO interface. The corresponding diffraction pattern obtained by the FFT pattern of the HRTEM images of the (c) ZnO NW branches, (d) the interface, and (e) the PTO core.

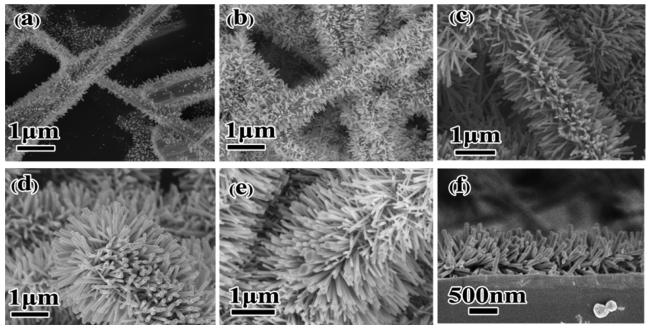

Figure 3. Growth manipulation of the PTO/ZnO nanocomposite using different reaction times: (a) 0.5 h; (b) 1 h; (c) 2 h; (d) 4 h; (e) 6 h. (f) Cross-sectional SEM image of the interface between the hybrids and substrate.

hardly able to grow between the PTO cores and poly(ethylene terephthalate) (PET) substrate.

The optical characteristics of the PTO NWs and PTO/ZnO nanocomposite were investigated by PL spectroscopy at room temperature where a He−Cd laser with 325 nm wavelength was used as the excitation source. The samples display a relatively weak UV emission peak centered at 384 nm and a strong and broad visible emission centered at 623 nm, whereas PTO NWs demonstrate no PL emission response (Figure S4 in the SI). The UV emission peak originates from a direct band excitation, and visible PL emission is typically assigned to the interstitial oxygen of ZnO synthesized by a hydrothermal method.[31] In order to test the bending effect on the PL properties of the as-synthesized composite, the sample was subjected to a bending force and excitation simultaneously. The photograph of the flexible PET substrate grown with a PTO/ZnO nanocomposite (Figure S5 in the SI) shows that the sample was highly flexible and robust, which could help it endure large deformation without cracking. Figure 4a shows the PL emission spectra from the deformed PTO/ZnO nanocomposite measured under different bending curvatures. As indicated in Figure 4a, the intensity of UV and visible emission shows an obvious increasing trend when the bending central angle is increased from $\alpha = 0°$ (unbent) to $\alpha = 190°$. The enhancement of the visible emission intensity might originate from the increasing amounts of defects due to deformation of the samples when a bending load is applied. No shift or splitting of the UV emission peaks is observed when the samples are bent, which indicates that there is no change of the photon energy for the UV emission induced by lattice strain in the ZnO NWs.[32] As depicted in the inset of Figure 4b, when the substrate was bent and stretched under a certain curvature, the core PTO NW whose bottom side is directly attached to the substrate undertook a corresponding deformation, whereas vertically branched ZnO NWs on the up side of the PTO NW were hardly affected. The intensity ratio of the UV-to-visible emission (I_{UV}/I_{vis}) was calculated to eliminate the problem of normalization of the intensity values. Figure 4b shows the plot of the ratio I_{UV}/I_{vis} as a function of the bending central angle. It can be observed that a clear transition of two linear-fitting regions appears in the curve for I_{UV}/I_{vis}, where the intensity ratio varies slowly at low bending curvatures but sharply increases when $\alpha > 130°$. This indicates that the bending

dx.doi.org/10.1021/am5009024 | ACS Appl. Mater. Interfaces 2014, 6, 10935−10940

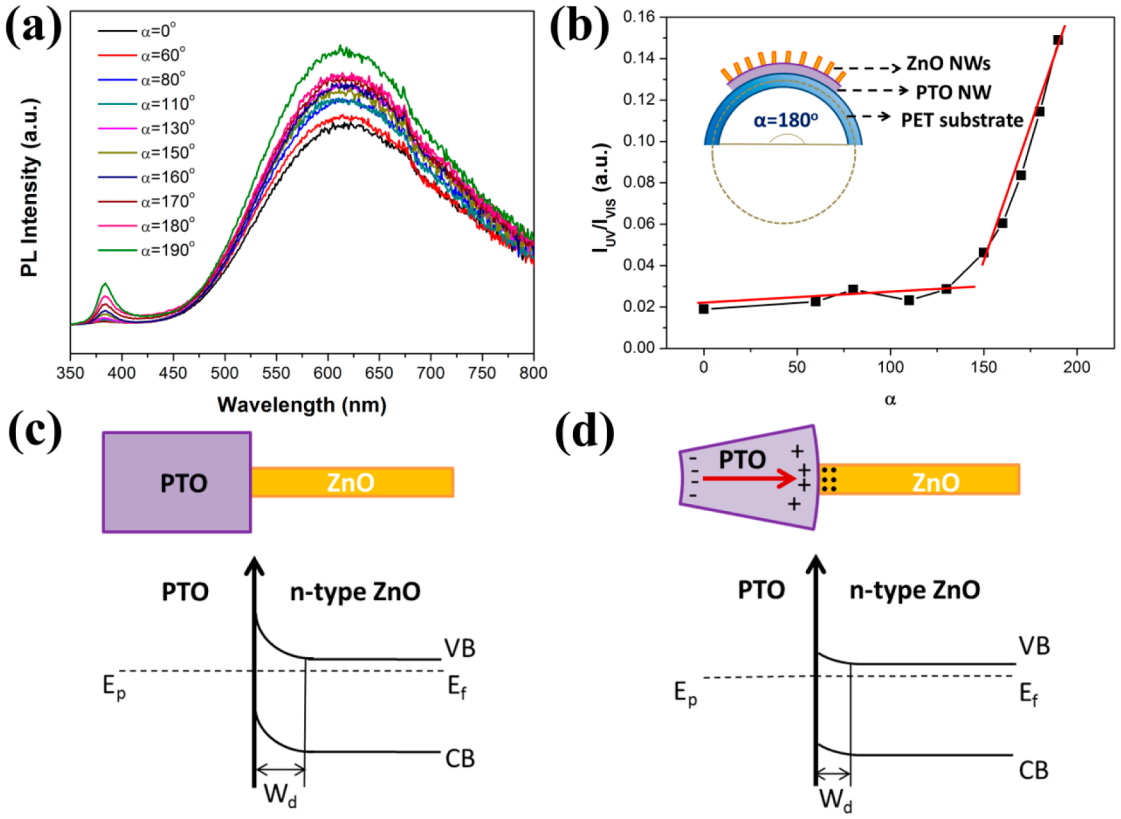

Figure 4. PL study of the bending sample. (a) PL spectra of a PTO/ZnO nanocomposite on a flexible PET substrate bent to different curvatures (α is the central angle of the bending circle, and $\alpha = 0°$ represents for the unbent sample). (b) Intensity ratio curve of the UV emission (at 384 nm) and the visible emission (at 623 nm) as a function of the bending central angle. The red lines indicate linear fitting areas. The inset shows the schematic depiction for the cross-sectional structures of the bending sample at α =180°. Schematic depictions of the PTO/ZnO nanocomposite and its corresponding potential energy profiles (c) at the original equilibrium state and (d) at the bending condition.

enhancement effect has a critical bending curvature at $\alpha = 130°$; in other words, the PL intensity of UV emission in the composite could be largely improved when the bending angle ranged from $\alpha = 130°$ to 190°. However, I_{UV}/I_{vis} tends to decline when the bending angle is further increased to 220° (as shown in Figure S6 in the SI), indicating that $I_{UV}/I_{vis} = 0.15$ at $\alpha = 190°$ is the maximum value (about 8 times that at $\alpha = 0°$). Thus, the PTO/ZnO nanocomposite displays a high level of flexibility and presents a linear correlation between the bending curvature and PL intensity of the composite, which makes them attractive for potential applications in bending sensors.

We attempted to explain the observed results by the polarization effect originating from the ferroelectric/semiconductor interface, as simply depicted in Figure 4c,d. Because the PTO/ZnO nanocomposite is free of bending, the interface will be governed by the alignment of the polarization potential E_p of the ferroelectric material with the electrochemical potential Fermi level E_F of the semiconductor (Figure 4c). Through the formation of an effective interface, the band structure of the ZnO NW bended upward and a surface depletion region formed through the accumulation of positively charged oxygen vacancies near the surface of the ZnO NW.[23] When a bending force is loaded on the PTO NW, as schematically shown in Figure 4d, the core PTO NW undertook a corresponding deformation while the ZnO branch was not affected. Then, the outer and inner bending arc surfaces of the PTO NW, enduring stretching and compression on the two sides, would be charged positively and negatively via the polarization effect, respectively.[33] Thus, a polarization field pointed toward the side of the ZnO NWs could be established along the axial direction of the PTO NW. Meanwhile, the positively bound charge at the ferroelectric/semiconductor interface will attract more negative charge on the surface of ZnO NWs, which can lower the bending degree of the energy band and the width of the depletion region (W_d). A similar effect was confirmed at the ZnO/electrolyte interface by applying an external positive electric field.[34] As a result, under UV laser illumination, the recombination of photogenerated electron−hole pairs in a bent PTO/ZnO nanocomposite could be promoted and hence led to an enhanced intensity of UV emission. However, as shown in Figure 4a, the value of I_{UV}/I_{vis} for the PTO/ZnO nanocomposites is not prominently changed with a small degree of bending. For one possible reason, enough bending deformation is necessary to realize the polarization potential effect on improving the PL emission, and the critical bending force was reached with bending degree $\alpha = 130°$ in this experiment. For another reason, the nanocomposites in this work were randomly arranged on the flexible substrates. When the bending degree was low, only the oriented ones parallel to the bending direction of the flexible substrate would take responsibility for improving the PL property. With an increase of the bending degree, the nanocomposites grown along other directions would subsequently begin to make considerable contributions to enhancing the PL emission intensity because they were loaded with enough component force along their axial direction.

dx.doi.org/10.1021/am5009024 | ACS Appl. Mater. Interfaces 2014, 6, 10935−10940

CONCLUSION

In summary, the PTO/ZnO nanocomposite consisting of ZnO branches with diameters of 30−200 nm and lengths of 200−2000 nm grown on a perovskite PTO NW has been successfully synthesized on a PET flexible substrate with a two-step hydrothermal method. It is found that the interfacial relationship between the (1000) plane of ZnO and the (101) plane of PTO with a low lattice mismatch can make a contribution to building an effective ferroelectric/semiconductor interface. Interestingly, when a bending stress was loaded onto the as-grown sample, the PL intensity of UV emission in the composite was enhanced with an increase of the bending curvature. It is proposed that the piezoelectric polarization field in the bent PTO NWs could lower the bending degree of the energy band for the ZnO NWs through the interface. The findings presented here may provide an opportunity for developing piezooptonic nanosensors by introducing ferroelectric/semiconductor interfaces into the nanomaterials.

ASSOCIATED CONTENT

Supporting Information

Experimental details, SEM images of the PTO NWs, PTO-implanted ZnO nanoparticle seeds, and samples obtained without coating a ZnO seed layer onto PTO NWs, PL spectra of the PTO core NW and PTO/ZnO nanocomposite excited by a 325-nm-wavelength laser at room temperature, photograph of the PET substrates grown with a PTO/ZnO nanocomposite under bending force, and the intensity ratio curve of I_{UV}/I_{vis} as a function of the bending central angle (α = 190−220°). This material is available free of charge via the Internet at http://pubs.acs.org.

AUTHOR INFORMATION

Corresponding Authors

*E-mail: renzh@zju.edu.cn. Fax: +86-571-87952341.
*E-mail: hgr@zju.edu.cn. Fax: +86-571-87952341.

Notes

The authors declare no competing financial interest.

ACKNOWLEDGMENTS

This work was financially supported by the National Natural Science Foundation of China (Grants 51232006, 51102212, and 51102208), the Program for Innovative Research Team in University of Ministry of Education of China (IRT13037), and the Fundamental Research Funds for the Central Universities (Grant 2014FZA4009).

REFERENCES

(1) Rørvik, P. M.; Grande, T.; Einarsrud, M. A. One-Dimensional Nanostructures of Ferroelectric Perovskites. *Adv. Mater.* **2011**, *23*, 4007−4034.
(2) Yang, P. D.; Yan, R. X.; Fardy, M. Semiconductor Nanowire: What's Next? *Nano Lett.* **2010**, *10*, 1529−1536.
(3) Yang, Y.; Zhang, H. L.; Zhu, G.; Lee, S. M.; Lin, Z. H.; Wang, Z. L. Flexible Hybrid Energy Cell for Simultaneously Harvesting Thermal, Mechanical, and Solar Energies. *ACS Nano* **2013**, *7*, 785−790.
(4) Fu, X. W.; Liao, Z. M.; Xu, J.; Wu, X. S.; Guo, W. L.; Yu, D. P. Improvement of Ultraviolet Photoresponse of Bent ZnO Microwires by Coupling Piezoelectric and Surface Oxygen Adsorption/Desorption Effects. *Nanoscale* **2013**, *5*, 916−920.
(5) Jiang, W. T.; Wu, C. T.; Sung, Y. H.; Wu, J. J. Room-Temperature Fast Construction of Outperformed ZnO Nanoarchitectures on Nanowire−Array Templates for Dye-Sensitized Solar Cells. *ACS Appl. Mater. Interfaces* **2013**, *5*, 911−917.
(6) Athauda, T. J.; Hari, P.; Ozer, R. R. Tuning Physical and Optical Properties of ZnO Nanowire Arrays Grown on Cotton Fibers. *ACS Appl. Mater. Interfaces* **2013**, *5*, 6237−6246.
(7) Wang, Z. L.; Song, J. Piezoelectric Nanogenerators Based on Zinc Oxide Nanowire Arrays. *Science* **2006**, *312*, 242−246.
(8) Qin, Y.; Wang, X. D.; Wang, Z. L. Microfibre−nanowire Hybrid Structure for Energy Scavenging. *Nature* **2008**, *451*, 809−813.
(9) Yang, P. H.; Xiao, X.; Li, Y. Z.; Ding, Y.; Qiang, P. F.; Tan, X. H.; Mai, W. J.; Lin, Z. Y.; Wu, W. Z.; Li, T. Q.; Jin, H. Y.; Liu, P. Y.; Zhou, J. C.; Wong, P.; Wang, Z. L. Hydrogenated ZnO Core−Shell Nanocables for Flexible Supercapacitors and Self-powered Systems. *ACS Nano* **2013**, *7*, 2617−2626.
(10) Dietrich, C. P.; Lange, M.; Klüpfel, F. J.; von Wenckstern, H.; Schmidt-Grund, R.; Grundmann, M. Strain Distribution in Bent ZnO Microwires. *Appl. Phys. Lett.* **2011**, *98*, 031105.
(11) Xiao, X.; Yuan, L. Y.; Zhong, J. W.; Ding, T. P.; Liu, Y.; Cai, Z. X.; Rong, Y. G.; Han, H. W.; Zhou, J.; Wang, Z. L. High-Strain Sensors Based on ZnO Nanowire/Polystyrene Hybridized Flexible Films. *Adv. Mater.* **2011**, *23*, 5440−5444.
(12) Liu, J. M.; Wu, W. W.; Bai, S.; Qin, Y. Synthesis of High Crystallinity ZnO Nanowire Array on Polymer Substrate and Flexible Fiber-Based Sensor. *ACS Appl. Mater. Interfaces* **2011**, *3*, 4197−4200.
(13) Wang, X.; Zhou, J.; Song, J.; Liu, J.; Xu, N.; Wang, Z. L. Piezoelectric Field Effect Transistor and Nanoforce Sensor Based on a Single ZnO Nanowire. *Nano Lett.* **2006**, *6*, 2768−2772.
(14) Gullapalli, H.; Vemuru, V. S. M.; Kumar, A.; Botello-Mendez, A.; Vajtai, R.; Terrones, M.; Nagarajaiah, S.; Ajayan, P. M. Flexible Piezoelectric ZnO−Paper Nanocomposite Strain Sensor. *Small* **2010**, *6*, 1641−1646.
(15) Xu, S.; Hansen, B. J.; Wang, Z. L. Piezoelectric-Nanowire-Enabled Power Source for Driving Wireless Microelectronics. *Nat. Commun.* **2010**, *1* (93), 1−8.
(16) Wang, Z. L.; Zhu, G.; Yang, Y.; Wang, S. H.; Pan, C. F. Progress in Nanogenerators for Portable Electronics. *Mater. Today* **2012**, *15*, 532−543.
(17) Scott, J. F. Applications of Modern Ferroelectrics. *Science* **2007**, *315*, 954−959.
(18) Chen, X.; Xu, S. Y.; Yao, N.; Shi, Y. 1.6 V Nanogenerator for Mechanical Energy Harvesting Using PZT Nanofibers. *Nano Lett.* **2010**, *10*, 2133−2137.
(19) Zhou, Z.; Tang, H. X.; Sodano, H. A. Vertically Aligned Arrays of $BaTiO_3$ Nanowires. *ACS Appl. Mater. Interfaces* **2013**, *5*, 11894−11899.
(20) Spanier, J. E.; Kolpak, A. M.; Urban, J. J.; Grinberg, I.; Ouyang, L.; Yun, W. S.; Rappe, A. M.; Park, H. K. Ferroelectric Phase Transitions in Individual Single-Crystalline $BaTiO_3$ Nanowrires. *Nano Lett.* **2006**, *6*, 735−739.
(21) Choi, T.; Lee, S.; Choi, Y. J.; Kiryukhin, V.; Cheong, S. W. Switchable Ferroelectric Diode and Photovoltaic Effect in $BiFeO_3$. *Science* **2009**, *324*, 63−66.
(22) Yi, H. T.; Choi, T.; Choi, S. G.; Oh, Y. S.; Cheong, S. W. Mechanism of the Switchable Photovoltaic Effect in Ferroelectric $BiFeO_3$. *Adv. Mater.* **2011**, *23*, 3403−3407.
(23) Wen, Z.; Li, C.; Wu, D.; Li, A. D.; Ming, N. B. Ferroelectric-Field-Effect-Enhanced Electroresistance in Metal/Ferroelectric/Semiconductor Tunnel Junctions. *Nat. Mater.* **2013**, *12*, 617−621.
(24) Jun, H.; Im, B.; Lee, K. H.; Lee, K. H.; Yang, I. K.; Jeong, Y. H.; Lee, J. S. Morphology Controlled Fabrication and Ferroelectric Properties of Vertically Aligned One-dimensional Lead Titanate Nanoarrays. *Nanotechnology* **2012**, *23*, 135602.
(25) Ren, Z. H.; Xu, G.; Liu, Y.; Wei, X.; Zhu, Y. H.; Zhang, X. B.; Lv, G. L.; Wang, Y. W.; Zeng, Y. W.; Du, P. Y.; Weng, W. J.; Shen, G.; Jiang, J. Z.; Han, G. H. $PbTiO_3$ Nanofibers with Edge-Shared TiO_6 Octahedra. *J. Am. Chem. Soc.* **2010**, *132*, 5572−5573.
(26) Xiao, Z.; Ren, Z. H.; Liu, Z. Y.; Wei, X.; Xu, G.; Liu, Y.; Li, X.; Shen, G.; Han, G. R. Single-crystal Nanofibers of Zr-doped New

Structured $PbTiO_3$: Hydrothermal Synthesis, Characterization and Phase transformation. *J. Mater. Chem.* **2011**, *21*, 3562.
(27) Xiao, Z.; Ren, Z. H.; Xia, Y.; Liu, Z. Y.; Xu, G.; Li, X.; Shen, G.; Han, G. R. Doping and Phase Transformation of Single-crystal Pre-perovskite $PbTiO_3$ Fibers with TiO_6 Edge-shared Octahedral. *CrystEngComm* **2012**, *14*, 4520−4524.
(28) Liu, Z. Y.; Ren, Z. H.; Xiao, Z.; Chao, C. Y.; Wei, X.; Liu, Y.; Li, X.; Xu, G.; Shen, G.; Han, G. R. Size-Controlled Single-Crystal Perovskite $PbTiO_3$ Nanofibers from Edge-Shared TiO_6 Octahedron Columns. *Small* **2012**, *8*, 2959−2963.
(29) Greene, L. E.; Law, M. D.; Tan, H.; Montano, M.; Goldberger, J.; Somorjai, G.; Yang, P. D. General Route to Vertical ZnO Nanowire Arrays Using Textured ZnO Seeds. *Nano Lett.* **2005**, *5*, 1231−1236.
(30) Guo, Z.; Chen, X.; Li, J.; Liu, J. H.; Huang, X. J. ZnO/CuO Hetero-Hierarchical Nanotrees Array: Hydrothermal Preparation and Self-Cleaning Properties. *Langmuir* **2011**, *27*, 6193−6200.
(31) Djurišić, A. B.; Leung, Y. H.; Tam, K. H.; Ding, L.; Ge, W. K.; Chen, H. Y.; Gwo, S. Yellow, and Orange Defect Emission from ZnO Nanostructures: Influence of Excitation Wavelength. *Appl. Phys. Lett.* **2006**, *88*, 103107.
(32) Liao, Z. M.; Wu, H. C.; Fu, Q.; Fu, X. W.; Zhu, X. L.; Xu, J.; Shvets, I. V.; Zhang, Z. H.; Guo, W. L.; Leprince-Wang, Y.; Zhao, Q.; Wu, X. S.; Yu, D. P. Strain Induced Exciton Fine-structure Splitting and Shift in Bent ZnO Microwires. *Sci. Rep.* **2012**, *2*, 452.
(33) Park, K. I.; Xu, S.; Liu, Y.; Hwang, G. T.; Kang, S. J. L.; Wang, Z. L.; Lee, K. J. Piezoelectric $BaTiO_3$ Thin Film Nanogenerator on Plastic Substrates. *Nano Lett.* **2010**, *10*, 4939−4943.
(34) Ghoshab, M.; Raychaudhuri, A. K. Electric Field Induced Reversible Control of Visible Photoluminescence from ZnO Nanoparticles. *Appl. Phys. Lett.* **2011**, *98*, 153109.